Localized states evolution and nitrides separation before crystallization in nitrogen incorporated GeTe: Evidence from ellipsometric spectra

S. Guo (郭爽),[1] M. J. Li (李梦姣),[1] Q. Q. Li (李欠欠),[1] Z. G. Hu (胡志高),[1,a)] T. Li (李涛),[2] L. C. Wu (吴良才),[2] Z. T. Song (宋志棠),[2] and J. H. Chu (褚君浩)[1]
[1]*Technical Center for Multifunctional Magneto-Optical Spectroscopy (ECNU), Shanghai and Department of Electronic Engineering, East China Normal University, Shanghai 200241, China*
[2]*State Key Laboratory of Functional Materials for Informatics, Shanghai Institute of Microsystem and Information Technology, Chinese Academy of Sciences, Shanghai 200050, China*

(Received 8 December 2016; accepted 4 April 2017; published online 18 April 2017)

The evolutions of localized states, dielectric functions, and electronic band structure for nitrogen (N) incorporated GeTe (NGT) as functions of temperature (210–660 K) and N concentration (0%–18%) have been investigated with the aid of temperature dependent spectroscopic ellipsometry experiments. The increased Urbach absorption energy, caused by band-tail localized states, can be attributed to the increment of structure defects with N concentration, which is generated from the N atoms bonding with Ge. Besides, the details of the dynamic crystallization process and the role of nitrogen in NGT films have been elucidated by the abnormal behavior of interband transition energy and the evolutions of surface morphology, namely, the nitrides separation before crystallization and the inhibition on GT crystallization. The dynamic crystallization process and the nitrogen behavior in NGT are of great significance for further study on the reliability and endurance of the NGT-based data storage devices. *Published by AIP Publishing.*
[http://dx.doi.org/10.1063/1.4980851]

Tellurium-based phase change materials are one of the most promising candidates for next-generation electronic and optical data storage. The phase change is obtained quickly and reversibly via a suitable sequence of Joule heating and melt-quench.[1–3] GeTe (GT) is of high technological interest being an end point of GeTe-Sb_2Te_3 (GST) pseudobinary tie line. Phase change memory (PCM) based on GT has been reported with larger resistance contrast, higher crystallization temperature, and faster SET operation than those of GST.[4,5] However, similar to the conventional GST, GT also exhibits a low amorphous (AM) phase stability and a high power consumption, which restrict its development in PCM. One of the solutions to modify the performances is via adding dopants into GT. It has been demonstrated that nitrogen (N) doping can solve the problems effectively.[6,7]

Previous researches indicated that nitrogen incorporated GeTe (NGT) has higher crystallization temperature, superior thermal stability, and better data retention ability, as compared with pure GT.[6–10] The crystal structure of NGT has been examined by X-ray diffraction (XRD) and transmission electron microscopy (TEM), which consists of amorphous (AM) GeN_x and rhombohedral (R) GeTe. However, for previous studies, the investigation on the crystal structure of NGT was basically done by testing the samples after thermal annealing, which can be obtained only from the final crystalline phase. The details of the dynamic crystallization process and the role of nitrogen in NGT are ambiguous. In addition, the modification of the band-tail localized states for GT by N incorporation has not been well understood up to date. The study of the properties mentioned above is significant for further applications of NGT-based data storage devices for its reliability and endurance.

To fill the gap of current studies, the evolutions of localized states and electronic band structure for NGT have been investigated with the aid of temperature dependent spectroscopic ellipsometry (SE) experiments. Besides, we elucidate the dynamic crystallization process and the role of nitrogen in NGT films, which can be concluded by analyzing the interband transition and the change of the surface morphology with increasing the temperature. Furthermore, the dielectric functions and electronic transitions of NGT films as functions of temperature and N concentration have been discussed in detail.

Amorphous GT and NGT films (~65 nm) were deposited on SiO_2/Si (100) substrates by reactive sputtering of a pure stoichiometric GT target using an N_2/Ar gas mixture with a background pressure of 2×10^{-4} Pa at room temperature. The N_2/Ar flow ratio was fixed at 0:100, 5:95, 10:90, and 20:80 in order. The nitrogen compositions were estimated to be around 0%, 8%, 12%, and 18% by X-ray photoemission spectroscopy (named GT, NGT8%, NGT12%, and NGT18%, respectively). Note that the compositions remain essentially unchanged after crystallization.[11] The temperature dependent SE measurements were performed in the photon energy range of 0.5–4.13 eV (300–2500 nm) at an incident angle of 70° by a vertical variable-angle SE (J. A. Woollam Co., Inc.). The samples were mounted into an Instec cell with liquid nitrogen as cooling accessories and argon as shielding gas. The temperature is varied from 210 to 660 K with a precision of about ±1 K. The window corrections were included as a part of the model during the fitting analysis. The surface morphologies of GT and NGT films at several typical temperatures were recorded through the 50× light microscope during the heating process

a)Author to whom correspondence should be addressed. Electronic mail: zghu@ee.ecnu.edu.cn. Tel.: +86-21-54345150. Fax: +86-21-54345119.

(210–660 K). Note that the samples were placed in a THMSE 600 heating/cooling stage (Linkam Scientific Instruments) with a fixed heating rate of 10 K/min.

SE is well known as an effective technique to determine the dielectric functions of various materials.[12–14] In the present work, a five-layered model (air/surface rough layer/NGT/SiO_2/Si) was used to extract the dielectric functions $[\tilde{\varepsilon}(E) = \varepsilon_1(E) + i\varepsilon_2(E)]$ of GT and NGT films with the WVASE32 software package (J. A. Woollam Co., Inc.). The dielectric functions for the AM phase were obtained by Tauc-Lorentz (TL) and Cody-Lorentz (CL) dispersion models. Both the models follow Kramers-Krönig transformation (KKT). The imaginary part of dielectric functions for the TL model can be written as:[15] $\varepsilon_{2TL}(E) = \frac{AE_nC(E-E_g)^2}{(E^2-E_n^2)^2+C^2E^2}\frac{1}{E}$, $(E \geq E_g)$ and $\varepsilon_{2TL}(E) = 0$, $(E < E_g)$. The CL model can be written as:[14,16] $\varepsilon_{2CL}(E) = \frac{E_1}{E}\exp\left(\frac{E-E_L}{E_u}\right)$, $0 < E\,(\leq E_g' + E_t)$ and $\varepsilon_{2CL}(E) = \frac{(E-E_g')^2}{(E-E_g')^2+E_p^2}\frac{A'E_n'C'E}{(E^2-E_n'^2)^2+C'^2E^2}$, $E > (E_g' + E_t)$. Here, $(E_t + E_g')$ represents the demarcation energy between Urbach tail transitions and band-to-band transitions. E_u corresponds to the weak Urbach absorption energy. E_1 is defined so that $\varepsilon_{2CL}(E)$ is continuous at $E = E_t$. E_p is a second transition energy separating the absorption onset from the Lorentz oscillator behavior. Note that E is the incident photon energy. Besides, A, E_n, C, and E_g in the TL model, as well as A', E_n', C', and E_g' in the CL model, represent the amplitude, peak transition energy, broadening term, and Tauc gap energy (optical bandgap energy) of the oscillator, respectively. One Lorentz oscillator and the Drude-like term for free carriers were added into the TL model to describe the crystalline samples.[17]

It is generally known that the TL model is widely used in amorphous semiconductors and also acceptable to describe the optical properties of indirect crystalline semiconductors.[12] However, the TL model ignores the weak Urbach absorption and localized state. In order to investigate the N incorporation effect on the band-tail localized state of GT, we employed the CL model to describe the dielectric functions in the absorption onset region.[14] It should be noted that it is not proper to employ the CL model in crystalline materials. This is mainly due to the impossibility to model the Urbach edge in the highly ordered crystalline phase contrary to the amorphous phase.[14] Therefore, the CL model was only employed in AM films. The fitting results of TL and CL models are compared and discussed in detail. In addition, to analyze the dynamic crystallization process, it is necessary to compare the change of the same parameter before and after crystallization. So the same model (TL) was applied to evaluate the ellipsometric spectra for both amorphous and crystalline phases.

Figs. 1(a) and 1(b) show the comparison of the experimental and calculated ellipsometric spectra (Ψ and Δ) for amorphous GT and NGT12% films at room temperature (300 K) obtained by TL and CL models described above. Both the models agree well with the experimental data. The insets depict a detailed view of Δ in the regions near and below the optical bandgap energy. It is seen that for Δ, the CL data match the experimental data in the absorption onset

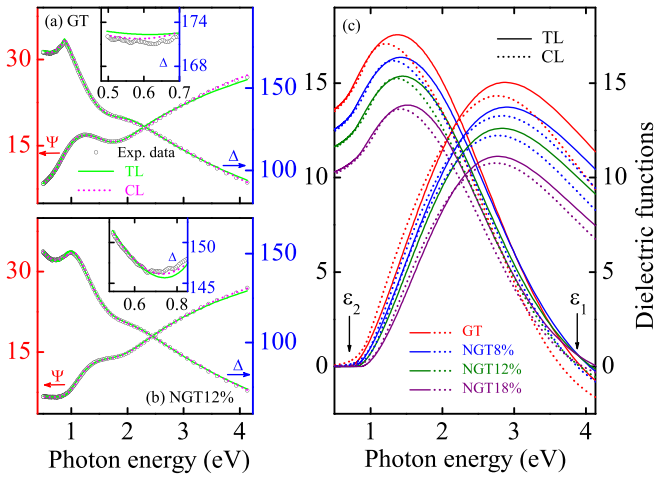

FIG. 1. Comparison of experimental (dots) and calculated (solid line for TL and dashed line for CL) ellipsometric spectra of Ψ and Δ for amorphous (a) GT and (b) NGT12% films. Note that the insets approach the Δ in the absorption onset region. (c) Comparison of the dielectric functions for amorphous GT and NGT films with different N concentrations obtained by TL and CL models.

regions better than TL data. Thus, it is reasonable to expect that the CL model is more appropriate to describe the dielectric functions of amorphous chalcogenide materials compared with the TL model. For ε_2, there is a non-zero absorption region below E_g, which corresponds to the localized states above the valence band in density of states, namely, the Urbach edge is governed by the valence band tail. These localized states can be considered as the result of "wrong" covalently bound atoms in amorphous chalcogenides, i.e., the so called valence alternation pairs VAPs.[18] The comparison of dielectric functions for GT and NGT calculated according to TL and CL models is shown in Fig. 1(c). The valence band of GT is dominated by Ge and Te p states, and minor contributions from the Ge s state. The peaks of ε_2 around 3 eV correspond to the strong optical absorption mainly associated with electronic transition from the Te and Ge p state.[19] The intensity trend of fitting results for the two models is in agreement, that is, the strength of ε_2 decreases with increasing N concentration.

The calculated parameters of TL and CL models are listed in Table I. It can be concluded that optical bandgap energy obtained from both TL and CL models for AM films at 300 K increases from 0.69 to 0.85 eV with the N concentration increasing to 18%. Besides, the bandgap energy for crystalline films obtained by the TL model elevated from 0.41 to 0.59 eV with increasing N concentration. The result is consistent with previous studies.[8,20] The broadening of the bandgap is significant to reducing the threshold current for a PCM.[21] A crucial important parameter is E_u, which is related to the weak Urbach absorption caused by transitions between band-tail states of one band. The increment of E_u (85.3 to 132 meV) is caused by the augmentation of band-tail localized states with increasing N concentration. It can be attributed to the increment of structure defects like dangling bonds derived from tellurium, which is generated from the N atoms bonding with Ge atoms. Therefore, the density of the VAPs increases, which will inevitably play the role in band-tail absorption.[22]

TABLE I. Dielectric function parameters of the TL and CL models for GT and NGT films are determined from the simulation of ellipsometric spectra. Note that d_s (d_s') and d_f (d_f') are the thickness of surface rough layers and films, respectively. The 95% reliability of the fitting parameters is given with (±).

Samples		GT	NGT8%	NGT12%	NGT18%
TL	d_s (nm)	5.97 ± 0.05	7.43 ± 0.04	6.11 ± 0.05	11.4 ± 0.09
	d_f (nm)	63.4 ± 0.07	66.1 ± 0.06	64.7 ± 0.08	62.8 ± 0.15
	A (eV)	114 ± 0.78	108 ± 0.69	101 ± 0.64	87.3 ± 0.81
	C (eV)	4.71 ± 0.03	4.67 ± 0.03	4.38 ± 0.02	3.86 ± 0.03
	E_n (eV)	3.40 ± 0.01	3.47 ± 0.008	3.26 ± 0.007	3.11 ± 0.007
	E_g (eV)	0.69 ± 0.002	0.74 ± 0.002	0.79 ± 0.002	0.85 ± 0.003
CL	d_s' (nm)	4.13 ± 0.10	6.21 ± 0.09	5.01 ± 0.10	10.1 ± 0.05
	d_f' (nm)	63.2 ± 0.12	66.8 ± 0.12	65.7 ± 0.13	64.0 ± 0.10
	A' (eV)	55.4 ± 0.68	57.6 ± 0.78	52.0 ± 0.70	42.4 ± 0.66
	C' (eV)	4.05 ± 0.04	4.49 ± 0.05	4.32 ± 0.05	3.91 ± 0.05
	E_n' (eV)	3.29 ± 0.01	3.40 ± 0.01	3.29 ± 0.01	3.17 ± 0.01
	E_g' (eV)	0.69 ± 0.005	0.74 ± 0.004	0.79 ± 0.004	0.85 ± 0.004
	E_p (eV)	0.47 ± 0.01	0.58 ± 0.01	0.61 ± 0.01	0.61 ± 0.01
	E_t (eV)	0.22 ± 0.07	0.24 ± 0.06	0.25 ± 0.03	0.26 ± 0.04
	E_u (meV)	85.3 ± 2.66	92.2 ± 3.53	101 ± 3.02	132 ± 4.40

The imaginary part ε_2 of the films at several typical temperatures is shown in Fig. 2. When the temperature reached a certain value, namely, the crystallization temperature (T_c), the main peaks corresponding to the high-energy electron transition show a remarkable narrowing, redshift, and intensity enhancement for all four samples. The transition corresponds to the structure change from amorphous to crystalline (AM-R). Moreover, an obvious enhancement of the Drude peak in the low energy region can be observed after crystallization. The significant difference of dielectric functions between amorphous and crystalline phases can be attributed to the increased degree of order in the crystalline phase.[12,13,17] The crystallization temperatures can be estimated to be 475, 505, 535, and 565 K for GT, NGT8%, NGT12%, and NGT18%, respectively. The elevated temperature with increasing N concentration can be ascribed to the existence of nitrides (GeN_x) in NGT films. It indicates that the existence of nitrides inhibits the structural evolution for the nucleation process and improves the thermal stability of the chalcogenide-based phase change materials, which is in accordance with previous studies.[7–10,20] After N incorporation, interfaces will form between GeTe and GeN_x, which can produce inhomogeneous nucleation sites and increase the nucleation rate.[20,23] Furthermore, the intensities of ε_2 for NGT8%, NGT12%, and NGT18% films in the crystalline phase reduce to about three quarters, one half, and one third of that for crystalline GT, respectively. The strength weakening degree is improved by increasing the N concentration. So it can be concluded that with the increasing N concentration, the strength of ε_2 decreases in both amorphous [Fig. 1(c)] and crystalline (Fig. 2) phases. This phenomenon should be attributed to the increased degree of disorder in NGT films. Note that the amplitude of ε_2 keeps on increasing when the temperature is higher than T_c, which can be due to the slightly continuous crystallization with increasing temperature.

To clarify the dynamic crystallization process and N incorporation effects of GT, the thermal evolutions of interband electronic transition energy (E_n) for GT and NGT are plotted in Fig. 3. The evolutions of E_n can be divided into

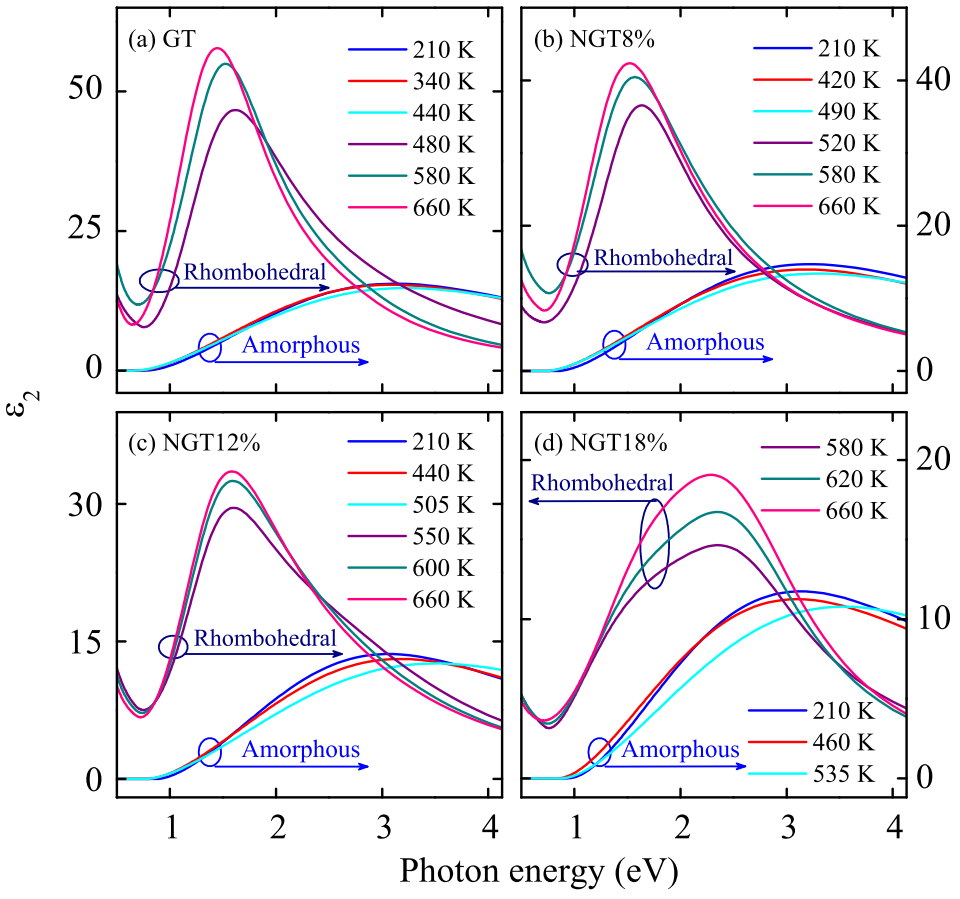

FIG. 2. Evolutions of the imaginary part (ε_2) for (a) GT, (b) NGT8%, (c) NGT12%, and (d) NGT18% films at several typical temperatures, respectively.

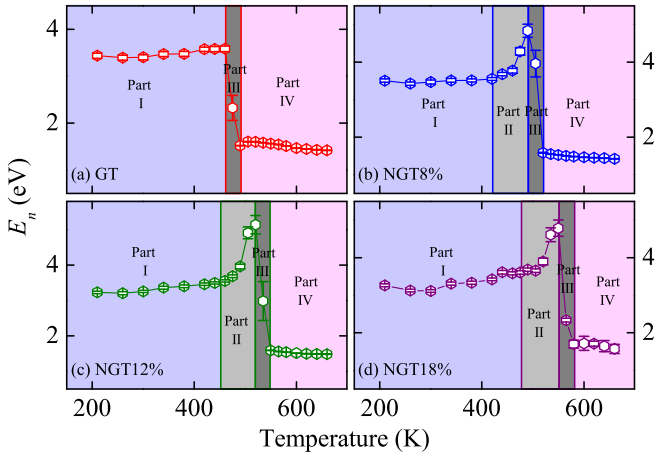

FIG. 3. Peak transition energy (E_n) evolutions of GT and NGT films with different N concentrations as a function of temperature.

four parts, i.e., Part I to Part IV. For Part I, the values of E_n are around 3.2 eV, and the values for Part IV are below 2 eV. The parameter E_n rapidly decreases through the narrow regions for Part III. Therefore, based on the preamble relevant discussion, Part I, III, and IV correspond to the amorphous structure, phase change regions, and crystalline phase of the samples, respectively. A similar evolutionary process of interband electronic transition energies for GT compared with NGT can be observed expect for Part II, which is an additional part for NGT films. The E_n for Part II in NGT films shows an ascending tendency, which appears before the phase change regions. The abnormal behavior can be attributed to the AM-GeN_x separation before crystallization, which has been proposed in previous studies.[20] Note that part of the incorporated N atoms already form nitrides GeN_x in the pristine film and the amount of nitrides increases constantly until they are separated from the compounds with the elevated temperature.[24] The AM-GeN_x precipitates to the grain boundaries hindering the crystallization process.[6,20,25,26] Therefore, it can be concluded that the separation of nitrides GeN_x is before GT crystallization instead of occurring during the phase change process for NGT films.

The dynamic crystallization process and the behavior of N also can be distinguished visually and real-timely by the evolution of surface morphology with increasing temperature. The surface morphologies for different crystalline natures of GT and NGT12% films were recorded through a 50× light microscope. Figs. 4(a)–4(c) and 4(d)–4(f) display the surface morphologies of GT at 300, 475, and 550 K, as well as those of NGT12% at 300, 530, and 600 K during the heating process. Figs. 4(a) and 4(d) are smooth surfaces for amorphous GT and NGT12%, which correspond to Part I in Figs. 3(a) and 3(c), respectively. For GT, as the temperature rises to about 470 K, the sample surface changes significantly, which corresponds to the beginning of crystallization. The surface morphology of GT at 475 K is shown in Fig. 4(b), which is an image during the phase changing process [Part III in Fig. 3(a)]. With further heating up, the GT film completes the crystallization basically at about 480 K. The surface morphology of GT at 550 K is shown in Fig. 4(c), which is an image of the crystalline phase [Part IV in Fig. 3(a)]. Similarly, for NGT12%, as the temperature rises to around

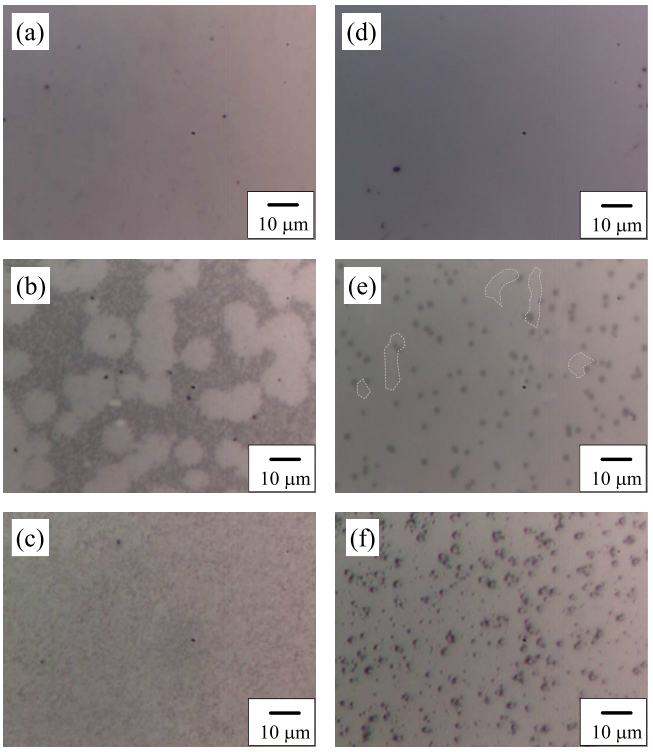

FIG. 4. Surface morphologies of GT and NGT12% films. (a)–(c) are images for GT at 300, 475, and 550 K corresponding to the amorphous structure, phase changing process, and crystalline phase, respectively. (d)–(f) are images for the NGT12% film at 300, 530, and 600 K corresponding to the amorphous structure, initial stage of crystallization, and crystalline phase, respectively. Note that several small crystalline regions are circled by dotted lines as examples.

490 K, the black spots start to appear on the smooth surface, which cannot be found in GT. With further increasing temperature, the black spots constantly increase and enlarge, which corresponds to the separation of AM-GeN_x before crystallization in NGT films. At 530 K, small crystalline regions begin to emerge. The surface morphology of NGT12% at 530 K is shown in Fig. 4(e), which corresponds to the initial stage of crystallization [Part II in Fig. 3(c)]. With further heating up, the crystallization completed for NGT12% at about 540 K. The surface morphology of NGT12% at 600 K is presented in Fig. 4(f), which is an image of crystalline NGT [Part IV in Fig. 3(c)]. The surface morphology evolution is in accordance with the change of interband electronic transition energies discussed in Fig. 3. Therefore, it is good information for the researches that the ellipsometry can be regarded as a new method to study the dynamic phase transformation process and the impurity behaviour for the phase change materials.

In summary, the modification of band-tail localized states and electronic band structure for GT by N incorporation has been studied by temperature dependent spectroscopic ellipsometry experiments. Furthermore, the details of the dynamic crystallization process and the role of nitrogen in NGT films have been elucidated, namely, the nitrides (AM-GeN_x) separation before crystallization and the inhibition on GT crystallization. This phenomenon can be concluded by the abnormal behavior of interband transition energy and the evolutions of surface morphology. The dynamic phase change process and the behavior of nitrogen

in NGT are significant for further study on the reliability and endurance of the NGT-based data storage devices.

This work was financially supported by the Major State Basic Research Development Program of China (Grant Nos. 2013CB922300 and 2011CB922200), Natural Science Foundation of China (Grant Nos. 61674057, 11374097, 61376129, and 61227902), Projects of Science and Technology Commission of Shanghai Municipality (Grant Nos. 15JC1401600 and 14XD1401500), and Program for Professor of Special Appointment (Eastern Scholar) at Shanghai Institutions of Higher Learning.

[1]G. I. Meijer, Science **319**, 1625 (2008).
[2]M. Wuttig and N. Yamada, Nat. Mater. **6**, 824 (2007).
[3]M. H. R. Lankhorst, B. W. S. M. M. Ketelaars, and R. A. M. Wolters, Nat. Mater. **4**, 347 (2005).
[4]G. Bruns, P. Merkelbach, C. Schlockermann, M. Salinga, M. Wuttig, T. D. Happ, J. B. Philipp, and M. Kund, Appl. Phys. Lett. **95**, 043108 (2009).
[5]S. Raoux, H.-Y. Cheng, M. A. Caldwell, and H.-S. P. Wong, Appl. Phys. Lett. **95**, 071910 (2009).
[6]K.-H. Kim, S.-J. Choi, J.-G. Chung, J.-H. Lee, and S. Heo, Jpn. J. Appl. Phys., Part 1 **49**, 061801 (2010).
[7]C. Peng, L. C. Wu, F. Rao, Z. T. Song, X. L. Zhou, M. Zhu, B. Liu, D. N. Yao, S. L. Feng, P. X. Yang, and J. H. Chu, Scr. Mater. **65**, 327 (2011).
[8]C. Peng, L. C. Wu, Z. T. Song, X. L. Zhou, M. Zhu, F. Rao, B. Liu, and S. L. Feng, J. Non-Cryst. Solids **358**, 2416 (2012).
[9]R. Fallica, E. Varesi, L. Fumagalli, S. Spadoni, M. Longo, and C. Wiemer, Phys. Status Solidi RRL **7**, 1107 (2013).
[10]K. Darmawikarta, S. Raoux, S. G. Bishop, and J. R. Abelson, Appl. Phys. Lett. **105**, 191903 (2014).
[11]A. V. Kolobov, P. Fons, B. Hyot, B. André, J. Tominaga, Y. Tamenori, H. Yoshikawa, and K. Kobayashi, Appl. Phys. Lett. **100**, 061910 (2012).
[12]S. Guo, X. J. Ding, J. Z. Zhang, Z. G. Hu, X. L. Ji, L. C. Wu, Z. T. Song, and J. H. Chu, Appl. Phys. Lett. **106**, 052105 (2015).
[13]S. Guo, L. P. Xu, J. Z. Zhang, Z. G. Hu, T. Li, L. C. Wu, Z. T. Song, and J. H. Chu, Sci. Rep. **6**, 33639 (2016).
[14]J. Orava, T. Wagner, J. Sik, J. Prikryl, M. Frumar, and L. Benes, J. Appl. Phys. **104**, 043523 (2008).
[15]G. E. Jellison, Jr. and F. A. Modine, Appl. Phys. Lett. 69, 371 (1996); **69**, 2137 (1996).
[16]A. S. Ferlauto, G. M. Ferreira, J. M. Pearce, C. R. Wronski, R. W. Collins, X. Deng, and G. Ganguly, J. Appl. Phys. **92**, 2424 (2002).
[17]K. Shportko, S. Kremers, M. Woda, D. Lencer, J. Robertson, and M. Wuttig, Nat. Mater. **7**, 653 (2008).
[18]H. Fritzsche, J. Phys. Chem. Solids **68**, 878 (2007).
[19]B. Huang and J. Robertson, Phys. Rev. B **85**, 125305 (2012).
[20]C. Peng, P. X. Yang, L. C. Wu, Z. T. Song, F. Rao, S. N. Song, D. Zhou, and J. H. Chu, J. Appl. Phys. **113**, 034310 (2013).
[21]W. Welnic, A. Pamungkas, R. Detemple, C. Steimer, S. Blugel, and M. Wuttig, Nat. Mater. **5**, 56 (2006).
[22]B. Huang, Phys. Status Solidi B **252**, 431 (2015).
[23]Y. Saito, Y. Sutou, and J. Koike, Appl. Phys. Lett. **100**, 231606 (2012).
[24]M.-C. Jung, Y. M. Lee, H.-D. Kim, M. G. Kim, and H. J. Shin, Appl. Phys. Lett. **91**, 083514 (2007).
[25]R. Kojima, S. Okabayashi, T. Kashihara, K. Horai, T. Matsunaga, E. Ohno, N. Yamada, and K. Ohta, Jpn. J. Appl. Phys., Part 1 **37**, 2098 (1998).
[26]S. Privitera, E. Rimini, C. Bongiorno, A. Pirovano, and R. Bez, Nucl. Instrum. Methods Res., Sect. B **257**, 352 (2007).